Gas-phase diagnoses in catalytic chemical vapor deposition (hot-wire CVD) processes

Gas-phase Diagnoses in Catalytic Chemical Vapor Deposition (Hot-Wire CVD) Processes

Hironobu Umemoto[1,2],

[1] Faculty of Engineering, Shizuoka University, Johoku, Naka, Hamamatsu, Shizuoka 432-8561, Japan

[2] Japan Science and Technology Agency, CREST, Sanbancho, Chiyoda, Tokyo 102-0075, Japan

E-mail address: thumemo@ipc.shizuoka.ac.jp

Abstract

Radical species play key roles in chemical vapor deposition (CVD) processes, including catalytic CVD (hot-wire CVD), and evaluating their densities in the gas phase is important in understanding the underlying mechanisms and controlling the processes. There are many diagnosis techniques to detect radical species. Among them, photon-in-photon-out techniques, including one- and two-photon laser-induced fluorescence and photo-absorption, can be utilized under the low vacuum conditions typical in CVD processes. Highly sensitive, quantitative, state-specific, real-time, and non-intrusive detection is possible with these techniques; even spatial resolution can be obtained in some cases. At the same time, however, we should know the drawbacks and the limitations of such techniques. A compilation of the radical species detected so far in catalytic CVD processes is presented in a table.

Keyword

catalytic chemical vapor deposition (Cat-CVD), hot-wire chemical vapor deposition (HW-CVD), free radical, laser spectroscopy, mass spectrometry

1. Introduction

There is growing interest in the catalytic chemical vapor deposition (hot-wire chemical vapor deposition or HW-CVD) technique [1,2]. In this technique, material gases are decomposed on heated metal wire surfaces, and functional films can be prepared with high deposition rates without plasma damage. It is easy to scale up for large-area deposition. This technique can also be used to generate high density radicals for surface treatment.

There are three stages in catalytic CVD processes. The first stage is the catalytic decomposition of material gas molecules on hot wire surfaces. For example, H_2 molecules are decomposed into H atoms and SiH_4 molecules are decomposed into Si and H atoms. The free radicals thus produced are transported to the substrate surfaces, and during the transportation, chemical reactions as well as translational and rotational relaxation may take place. For example, H atoms may react with SiH_4 to produce SiH_3 radicals. This is the second stage. The final third stage is the deposition of the radical species. Si and SiH_3 may deposit on the substrate surfaces to form Si films. Etching of the deposited films by radical species may also take place.

It is important to identify the radical species in the gas phase in order to understand the deposition mechanisms and control the processes, because these radicals are the direct products of the decomposition processes on the catalyst surface and the direct precursors of the deposited film [3]. Of course, it is also important to investigate the reactions on both the catalyst and substrate surfaces. However, diagnoses on surfaces, especially on the glittering hot catalyst surfaces, are more difficult than those in the gas phase. Gas-phase diagnosis is easier and can be a starting point to understand the whole mechanism.

Radical species are highly reactive because they have unpaired electrons. This means that radical densities cannot be high; if we produce radicals in high density, they will react with

each other and be annihilated, although the recombination reactions of two atomic radicals require third bodies and are slow at low pressures. The typical densities of those radical species which play important roles in CVD processes are 10^{10}-10^{13} cm^{-3}, although the densities of some atomic species can be more than 10^{16} cm^{-3} [4].

2. Radical detection techniques

Because the densities of the radicals are so low, it is necessary to employ highly sensitive techniques to detect them. Laser spectroscopic and mass spectrometric techniques are widely used in the diagnosis of CVD processes [3]. In any diagnosis technique to detect ground-state species, we need input and output. The input may be photons, electrons, or ions. In laser spectroscopic techniques, we use photons as input. In mass spectrometric techniques, we can use photons, electrons, or ions as input, and ions as output. Under typical CVD conditions, the pressure is too high for electrons and ions to fly several centimeters without colliding. In other words, sampling is necessary. On the other hand, in photon-in-photon-out techniques, such as laser-induced fluorescence (LIF), the limitations on chamber pressure conditions are much looser and *in situ* detection is possible.

One of the merits of mass spectrometric techniques, besides their high sensitivity, is that one apparatus can be used to detect many kinds of species [3]. However, this can also be a weak point: parent molecules, which are usually much more abundant than radicals, may be decomposed to produce fragment ions. Several ionization techniques have been proposed to overcome this problem, including photo-ionization, threshold-ionization, and ion-attachment. The photo-ionization technique is further classified into single-photon and multi-photon ones. In the threshold-ionization technique, the energy of the impact electron is reduced so as not to ionize the parent molecules. Ion-attachment is one of the softest ionization methods, and no

fragmentation is expected [5].

There are many kinds of laser spectroscopic techniques, such as one-photon laser-induced fluorescence (LIF), two-photon LIF, photo-absorption, resonance-enhanced multiphoton ionization (REMPI), and cavity ringdown spectroscopy (CRDS). The first step in each of these techniques is photo-absorption, which is species- and state-specific. This is again a double-edged sword, because photo-absorption takes place only at particular wavelengths and this is too specific to apply to many kinds of species. Thus, in general, only one species can be detected by one setup. Then, in order to clarify all the mechanisms of CVD processes, a number of techniques must be combined.

Conventional light sources can be used to detect radicals, but lasers are more suitable, because lasers are intense, tunable, coherent, monochromatic, directional, and less divergent. Time-resolved measurements and outputs in ultraviolet and vacuum ultraviolet regions can easily be obtained with pulsed lasers. Synchrotron radiation is another option, but this is less handy.

Table 1 summarizes the radical species detected in catalytic CVD (HW-CVD) processes by laser spectroscopic and mass spectrometric techniques. The results of the detection of H atoms in the catalytic decomposition of H_2 are not included since they have been reviewed recently [4]. As for organosilicon compounds, only the radicals produced directly on hot wire surfaces are listed. In the following discussion, the principles of three typical laser spectroscopic techniques, one- and two-photon LIF and photo-absorption, will be presented. For further experimental details, as well as those for other techniques such as mass spectrometric ones, the readers should refer to the original papers listed in Table 1.

3. Fundamentals in laser spectroscopic techniques

3.1 One-photon laser-induced fluorescence

In laser-induced fluorescence, the lower-state, usually ground-state, species are excited to one of the upper excited states and spontaneous emission is observed. The firsts step, as for other photon-in techniques, is photo-absorption. The rate of photo-absorption is given by:

$$W_{12} = B_{12}\rho(\nu), \tag{1}$$

where B_{12} is the Einstein B coefficient and $\rho(\nu)$ is the energy density of photons at the frequency of ν. The transition rate from the upper state, state 2, to the lower state, state 1, is:

$$W_{21} = B_{21}\rho(\nu) + A_{21}, \tag{2}$$

where A_{21} is the Einstein A coefficient. The first and second terms correspond to induced radiation and spontaneous radiation, respectively. Theoretical considerations give the following relationships [64]:

$$g_1 B_{12} = g_2 B_{21}, \tag{3}$$

$$A_{21} = \frac{8\pi h \nu^3}{c^3} B_{21}, \tag{4}$$

where g_1 and g_2 are the statistical weights of the lower and upper levels, while h and c have their usual meanings.

A two-level system is usually enough to model LIF. In general, there may be more than two decay processes if just one level is excited. For example, both ground-state Si($3s^2 3p^2\ ^3P_J$) and excited-state Si($3s^2 3p4s\ ^3P_J$) have three spin-orbit sublevels. When we excite $3s^2 3p^2\ ^3P_1$ to $3s^2 3p4s\ ^3P_1$, it may decay not only to $3s^2 3p^2\ ^3P_1$ but also to $3s^2 3p^2\ ^3P_0$ and $3s^2 3p^2\ ^3P_2$. In addition, collisional state mixing among the excited states, such as intramultiplet mixing, may take place. In many cases, however, it is possible to select what can be regarded as a two-level system, consisting of just one lower state and one upper state. For example, if we excite Si($3s^2 3p^2\ ^3P_1$) to Si($3s^2 3p4s\ ^3P_0$), fluorescence only to $3s^2 3p^2\ ^3P_1$ is allowed and this can be regarded as a two-level system [39]. When we use nanosecond lasers, state mixing, including

the rotational mixing for molecular species, is minor during the laser pulse when the pressure is less than 100 Pa. It should be noted, however, that the radiative lifetime of the upper state is sometimes long enough to be collisionally quenched. In general, the effect of predissociation must also be taken into account when molecular species are detected.

When we detect molecular radicals, such as SiH, NH, OH, and PH, the radiative lifetimes of the excited states are usually much longer than the duration time of nanosecond laser pulses and spontaneous radiation during the laser pulse can be ignored [30,34,36,37,39,61]. After the laser pulse, these systems cannot be regarded as two-level ones, but that does not matter unless the fluorescence is highly dispersive. As far as we detect these radicals by exciting to the vibrational ground states of the first electronically excited states, it is not necessary to take into account the effect of predissociation. The rotational period of the molecules is much shorter than the radiative lifetime and the induced fluorescence may be assumed to be isotropic. This is in contrast to the detection of atomic species with short radiative lifetimes. For example, when we excite Si($3s^2 3p^2\ ^3P_0$) to Si($3s^2 3p4s\ ^3P_1$), it is necessary to take into account the anisotropy of the fluorescence [39]. In this section, we will restrict the discussion to the detection of molecular species with long radiative lifetimes, using nanosecond pulsed lasers.

The differential of the upper-state population, N_2, should be given by:

$$\frac{dN_2}{dt} = \rho(\nu)B_{12}N_1 - \{\rho(\nu)B_{21} + A_{21} + \sum k_i n_i\}N_2 = \rho(\nu)B_{12}N - \{\rho(\nu)(B_{12} + B_{21}) + A_{21} + \sum k_i n_i\}N_2, \quad (5)$$

where N_1 is the lower-state population and $N(=N_1+N_2)$ is the population of the lower state before excitation, which is what we would like to know. The rate constant for the quenching of the upper state and the number density of the quenching molecules are represented by k_i and n_i. If we assume that the laser pulse is rectangular in shape and the duration time is Δ, the upper-state

population just after the laser pulse is given by:

$$N_2(\Delta) = \frac{\rho(\nu)B_{12}N\left(1-\exp\left[-\left\{\rho(\nu)(B_{12}+B_{21})+A_{21}+\sum k_i n_i\right\}\Delta\right]\right)}{\rho(\nu)(B_{12}+B_{21})+A_{21}+\sum k_i n_i}. \quad (6)$$

The time-integrated LIF intensity should be proportional to:

$$I_{LIF} \propto N_2(\Delta)\varphi = \frac{\rho(\nu)A_{21}B_{12}N\left(1-\exp\left[-\left\{\rho(\nu)(B_{12}+B_{21})+A_{21}+\sum k_i n_i\right\}\Delta\right]\right)}{\{\rho(\nu)(B_{12}+B_{21})+A_{21}+\sum k_i n_i\}(A_{21}+\sum k_i n_i)}. \quad (7)$$

Here, φ is the quantum yield of the fluorescence. If the laser is intense enough to saturate the transitions, the LIF intensity should be:

$$I_{LIF} \propto \frac{g_2 A_{21} N}{(g_1+g_2)(A_{21}+\sum k_i n_i)}, \quad (8)$$

and independent of $\rho(\nu)$. If the laser intensity is weak, that should be:

$$I_{LIF} \propto \frac{\rho(\nu)A_{21}B_{12}N[1-\exp\{-(A_{21}+\sum k_i n_i)\Delta\}]}{(A_{21}+\sum k_i n_i)^2}, \quad (9)$$

and proportional to $\rho(\nu)$. In both cases, the LIF intensity is proportional to N and it is easy to evaluate the *relative populations* under various conditions. It is also possible to determine the rotational state distributions since the radiative lifetimes, which are equivalent to $1/A_{21}$, the quenching rate constants, k_i, and the Hönl-London factors, which are proportional to B_{12}, have been reported for many species. The vibrational state distributions can also be determined if the Franck-Condon factors are known, but vibrationally excited radicals have not been identified in catalytic decomposition except for HCN, in which vibrationally excited CN has been detected [60].

Shown in Fig. 1 is an LIF spectrum of OH formed from H_2O on a heated Ir wire and a simulated one [37]. These spectra correspond to the (0,0) band of the $A\,^2\Sigma^+ - X\,^2\Pi$ transition. The laser intensity was low enough not to saturate the transitions. In the simulation, the rotational temperature was assumed to be 350 K. This temperature is typical when the distance from the wire is several centimeters.

3.2 Evaluation of the absolute densities in one-photon laser-induced fluorescence

The absolute densities of radical species can be evaluated in LIF. Excited species are produced along the optical path. Among them, only those in a small volume, V, can be detected. When the fluorescence is isotropic, only a part of the fluorescence, in a solid angle of Ω, can be detected. In addition, the absolute sensitivity of the detector, typically a photomultiplier tube, η, must be known. Fortunately, the product of these parameters, $V\Omega\eta$, can be evaluated by measuring the Rayleigh scattering intensity caused by rare gas atoms, such as Ar. Under saturated conditions, the LIF intensity in energy unit is given by:

$$I_{LIF} = \frac{g_2 A_{21} N h\nu}{(g_1 + g_2)(A_{21} + \sum k_i n_i)} V\eta \frac{\Omega}{4\pi}. \tag{10}$$

The Rayleigh scattering intensity is expressed by:

$$I_{Rayleigh} = \frac{N_0 \sigma E_L V\Omega\eta}{S_L}. \tag{11}$$

Here, N_0 is the rare gas atom density, E_L is the laser pulse energy, S_L is the cross section of the laser beam, and σ is the differential cross section for Rayleigh scattering, which can be calculated from the refractive index. Then, the absolute density can be evaluated by the following equation:

$$N = \frac{g_1 + g_2}{g_2} \frac{A_{21} + \sum k_i n_i}{A_{21}} \frac{4\pi}{h\nu} \frac{N_0 \sigma E_L}{S_L} \frac{I_{LIF}}{I_{Rayleigh}}. \tag{12}$$

Usually, we select a spectral line which does not overlap others. In other words, the population of just one rotational state is determined. To evaluate the total population, the rotational state distribution must be known. This can be done by analyzing the LIF spectrum as shown in Fig.1. If information on the absolute values of B_{12} is available, it is also possible to determine the absolute densities by comparing the intensities under the condition that the LIF intensity is proportional to the laser intensity.

3.3 Single-path photo-absorption

The one-photon LIF technique can also be applied to the detection of H, O, and N atoms,

although a vacuum ultraviolet (VUV) laser must be used for these atoms [4,32-37,65]. The wavelengths should be 121.6, 130.2, and 120.1 nm, respectively. In such systems, the photo-absorption technique is useful to evaluate the absolute densities. A single path is enough because of their large absorption coefficients. One problem is that the well-known Lambert-Beer law, $Tr = \exp(-\varepsilon Nl)$, cannot be used. Here, Tr is the transmittance, ε is the absorption coefficient, and l is the path length. This relationship can be applied only when the absorption spectrum is much broader than the bandwidth of the incident beam; in VUV absorption by atoms, the absorption spectrum is too sharp. There are three types of spectral broadening: natural, Doppler, and collisional. In typical CVD conditions (below 1 kPa and over 300 K), the natural and collisional broadenings are much narrower than the Doppler broadening, which is caused by the translational motion of the absorbing species and expressed by the following equation [64].

$$\varepsilon(\nu-\nu_0)=\left(\frac{m}{2\pi k_{\mathrm{B}}T}\right)^{1/2}\frac{g_2c^3}{8\pi g_1\nu_0^{\,3}\tau}\exp\left\{-\frac{mc^2(\nu-\nu_0)^2}{2k_BT\nu_0^{\,2}}\right\}. \qquad (13)$$

Here, ν is the frequency of radiation, ν_0 is the frequency at the absorption peak, k_{B} is the Boltzmann constant, m is the mass of the molecule, and τ is the radiative lifetime of the upper state. T and c have their usual meanings. The general representation of the transmittance is given in [64]:

$$Tr(\nu_L)=\frac{\int I(\nu-\nu_L)\exp\{-\varepsilon(\nu-\nu_0)Nl\}d\nu}{\int I(\nu-\nu_L)d\nu}. \qquad (14)$$

Here, ν_{L} is the peak frequency of the laser and $I(\nu-\nu_{\mathrm{L}})$ represents the frequency distribution. If $I(\nu-\nu_{\mathrm{L}})$ is known, N can be evaluated by measuring $Tr(\nu_{\mathrm{L}})$ as a function of ν_{L}. In the detection of H atoms by the absorption of Lyman-α, a little modification is necessary because Lyman-α is an unresolved doublet due to spin-orbit interaction. In this case, the optical density, $\varepsilon(\nu-\nu_0)Nl$, must be expressed by a sum of two terms [4,65].

3.4 Two-photon laser-induced fluorescence

When the atomic density is very high neither one-photon LIF nor photo-absorption can be employed, because laser radiation may not reach the central part of the chamber. Two-photon LIF is suitable in such optically thick systems [4]. In this technique, the ground-state species are two-photon excited *via* a virtual state. For example, H(n=1) is excited to H(n=3) by laser radiation at 205.1 nm, where n is the principle quantum number. H(n=3) fluoresces Balmer-α at 656.3 nm, which can be monitored. Since VUV radiation is not used, it is not necessary to account for the effect of VUV absorption by molecular species. As for H atoms, the absolute density can be determined by measuring the signal intensity of a known amount of Kr [4]. This technique, however, cannot be applied in the presence of material gases which can be two-photon decomposed to produce H atoms, such as NH_3 and Si_2H_6.

In the detection of H atoms, the two-photon LIF technique to observe Balmer-α can be used in high-density systems and has spatial resolution. VUV LIF has the highest sensitivity, while the absolute densities can be determined by VUV absorption. By combining these techniques, it is possible to determine absolute densities under wide conditions [4].

3.5 Other laser spectroscopic techniques to cover the limitations of LIF

Because of its nature, LIF cannot be applied to species which dissociate after photo-absorption, such as CH_3 and SiH_3. In order to detect such species, resonance-enhanced multi-photon ionization (REMPI), cavity ringdown spectroscopy (CRDS), and tunable diode laser absorption spectroscopy (TDLAS) are useful. With the latter two techniques, absolute densities can also be determined. The REMPI technique typically involves a resonant single or multiple photon absorption to an electronically excited state followed by the absorption of another photon to ionize the intermediate state. Since focused laser beams are used and the ionization takes place

only near the focal point, spatial resolution can be achieved. REMPI is extremely sensitive when combined with a time-of-flight mass spectrometric technique. On the other hand, when used without mass selection, high vacuum is not required and the technique can be used under typical CVD conditions. Both pulsed and continuous-wave lasers can be used in CRDS. In both cases, we measure the time profiles of the laser intensity leaking from an optical cavity, which consists of two highly reflective mirrors. For continuous-wave lasers, the profiles are recorded just after the termination of the laser. In the presence of some absorbing species, the decay is faster than in their absence because of the additional losses caused by sample absorption, and it is possible to evaluate the column densities by measuring the decay time, or *ringdown time*. In TDLAS, a single mode diode laser is used. Most polyatomic radicals are infrared active and can be detected by absorption. Since the absorption coefficients of molecular species are much smaller than those of atoms, multi-path absorption is essential. The wavelength region is in the mid-infrared, 2.5-25 μm, which corresponds to the fundamental vibrational excitation.

LIF cannot be used in the presence of strong background emissions, which are inevitable in plasma processes. When we wish to detect radicals near a hot filament, strong black-body radiation also hinders the measurements. The three techniques discussed above, REMPI, CRDS, and TDLAS, can be used in the presence of background emissions.

4. Discussion and future prospects

CH_3 is considered to be one of the most dominant growth species in the diamond film deposition. The situation is similar in the deposition of amorphous and poly-crystalline silicon films, and SiH_3 should be the dominant precursor of these films. In both systems, H atoms play a critical role in the production of these radicals and in film growth [4]. The efficiency of

producing H atoms from H_2 in catalytic decomposition is higher than in typical glow plasma processes [4], and this high efficiency leads to the efficient production of CH_3 and SiH_3 in the gas phase. On the other hand, the production efficiencies of O and N atoms are low compared to plasma processes [32-36]. It should be stressed, however, that only ground-state atoms are produced in the catalytic decomposition of O_2 and N_2. In plasma processes, many metastable species, such as $O(^1D_2)$, $O_2(a^1\Delta_g)$, $N(^2D_J)$, and $N_2(A^3\Sigma_u^+)$ are produced, which may disturb the system.

In the catalytic decomposition of SiH_4, laser spectroscopic and mass spectrometric studies have revealed that the major products are Si and H atoms [3,38,39,42,43]. Similarly, P and H atoms are mainly produced in the decomposition of PH_3 on heated W [61,62]. On the other hand, the major products are NH_2 and H for NH_3 [30]. This may represent the weakness of the Si-H and P-H bonds compared to the N-H bonds. In the decomposition of H_2O, the production of OH and H is major at low catalyst temperatures, but H and O production becomes more dominant at high temperatures [37]. As for organosilicon compounds, selective and efficient decomposition is possible [51-57]. The decomposition paths are different from those in thermal decomposition. Organosilicon compounds are stable and much safer than SiH_4 and can be good source materials in the preparation of SiC and SiCN films.

Fundamental studies are important in the development of any technology and in the pioneering of new application fields. Laser spectroscopic techniques are useful and can be good tools for developing CVD technology. In order to apply spectroscopic techniques properly, however, we must have a correct knowledge of the principles and keep in mind the limitations.

Acknowledgement

The author is grateful to Professor Yujun Shi of the University of Calgary for making her results

available for use prior to publication and also for her valuable discussions.

References

[1] R. E. I. Schropp, Thin Solid Films 517 (2009) 3415.

[2] H. Matsumura, K. Ohdaira, Thin Solid Films 517 (2009) 3420.

[3] H. L. Duan, G. A. Zaharias, S. F. Bent, Curr. Opin. Solid State Mater. Sci. 6 (2002) 471.

[4] H. Umemoto, Chem. Vapor Deposition 16 (2010) 275.

[5] T. Morimoto, S. G. Ansari, K. Yoneyama, T. Nakajima, A. Masuda, H. Matsumura, M. Nakamura, H. Umemoto, Jpn. J. Appl. Phys. 45 (2006) 961.

[6] F. G. Celii, P. E. Pehrsson, H.-T. Wang, J. E. Butler, Appl. Phys. Lett. 52 (1988) 2043.

[7] W. L. Hsu, Appl. Phys. Lett. 59 (1991) 1427.

[8] F. G. Celii, J. E. Butler, J. Appl. Phys. 71 (1992) 2877.

[9] E. J. Corat, D. G. Goodwin, J. Appl. Phys. 74 (1993) 2021.

[10] K. L. Menningen, M. A. Childs, P. Chevako, H. Toyoda, L. W. Anderson, J. E. Lawler, Chem. Phys. Lett. 204 (1993) 573.

[11] J. Heinze, N. Heberle, K. Kohse-Höinghaus, Chem. Phys. Lett. 223 (1994) 305.

[12] H. Toyoda, M. A. Childs, K. L. Menningen, L. W. Anderson, J. E. Lawler, J. Appl. Phys. 75 (1994) 3142.

[13] M. A. Childs, K. L. Menningen, P. Chevako, N. W. Spellmeyer, L. W. Anderson, J. E. Lawler, Phys. Lett. A 171 (1992) 87.

[14] M. A. Childs, K. L. Menningen, H. Toyoda, Y. Ueda, L. W. Anderson, J. E. Lawler, Phys. Lett. A 194 (1994) 119.

[15] M. C. McMaster, W. L. Hsu, M. E. Coltrin, D. S. Dandy, J. Appl. Phys. 76 (1994) 7567.

[16] P. Zalicki, Y. Ma, R. N. Zare, E. H. Wahl, T. G. Owano, C. H. Kruger, Appl. Phys. Lett. 67 (1995) 144.

[17] P. Zalicki, Y. Ma, R. N. Zare, E. H. Wahl, J. R. Dadamio, T. G. Owano, C. H. Kruger, Chem.

Phys. Lett. 234 (1995) 269.

[18] E. H. Wahl, T. G. Owano, C. H. Kruger, P. Zalicki, Y. Ma, R. N. Zare, Diam. Relat. Mater. 5 (1996) 373.

[19] M. A. Childs, K. L. Menningen, L. W. Anderson, J. E. Lawler, J. Chem. Phys. 104 (1996) 9111.

[20] E. H. Wahl, T. G. Owano, C. H. Kruger, Y. Ma, P. Zalicki, R. N. Zare, Diamond Rel. Mater. 6 (1997) 476.

[21] V. Zumbach, J. Schäfer, J. Tobai, M. Ridder, T. Dreier, T. Schaich, J. Wolfrum, B. Ruf, F. Behrendt, O. Deutschman, J. Warnatz, J. Chem. Phys. 107 (1997) 5918.

[22] U. Lommatzsch, E. H. Wahl, T. G. Owano, C. H. Kruger, R. N. Zare, Chem. Phys. Lett. 320 (2000) 339.

[23] J. A. Smith, M. A. Cook, S. R. Langford, S. A. Redman, M. N. R. Ashfold, Thin Solid Films 368 (2000) 169.

[24] U. Lommatzsch, E. H. Wahl, D. Aderhold, T. G. Owano, C. H. Kruger, R. N. Zare, Appl. Phys. A 73 (2001) 27.

[25] J. A. Smith, E. Cameron, M. N. R. Ashfold, Y. A. Mankelevich, N. V. Suetin, Diamond Rel. Mater. 10 (2001) 358.

[26] J. A. Smith, J. B. Wills, H. S. Moores, A. J. Orr-Ewing, M. N. R. Ashfold, Y. A. Mankelevich, N. V. Suetin, J. Appl. Phys. 92 (2002) 672.

[27] Yu. A. Mankelevich, N. V. Suetin, J. A. Smith, M. N. R. Ashfold, Diamond Rel. Mater. 11 (2002) 567.

[28] J. Hirmke, F. Hempel, G. D. Stancu, J. Röpcke, S. M. Rosiwal, R. F. Singer, Vacuum 80 (2006) 967.

[29] J. Hirmke, A. Glaser, F. Hempel, G. D. Stancu, J. Röpcke, S. M. Rosiwal, R. F. Singer,

Vacuum 81 (2007) 619.

[30] H. Umemoto, K. Ohara, D. Morita, T. Morimoto, M. Yamawaki, A. Masuda, H. Matsumura, Jpn. J. Appl. Phys. 42 (2003) 5315.

[31] H. Umemoto, Y. Kashiwagi, K. Ohdaira, H. Kobayashi, K. Yasui, Thin Solid Films 519 (2011) 4429.

[32] H. Umemoto, Appl. Phys. Express 3 (2010) 076701.

[33] H. Umemoto, T. Funae, Y. A. Mankelevich, J. Phys. Chem. C 115 (2011) 6748.

[34] H. Umemoto, M. Moridera, J. Appl. Phys. 103 (2008) 034905.

[35] H. Umemoto, H. Kusanagi, J. Phys. D: Appl. Phys. 41 (2008) 225505.

[36] H. Umemoto, H. Kusanagi, K. Nishimura, M. Ushijima, Thin Solid Films 517 (2009) 3446.

[37] H. Umemoto, H. Kusanagi, Open Chem. Phys. J. 2 (2009) 32.

[38] J. Doyle, R. Robertson, G. H. Lin, M. Z. He, A. Gallagher, J. Appl. Phys. 64 (1988) 3215.

[39] Y. Nozaki, K. Kongo, T. Miyazaki, M. Kitazoe, K. Horii, H. Umemoto, A. Masuda, H. Matsumura, J. Appl. Phys. 88 (2000) 5437.

[40] Y. Nozaki, M. Kitazoe, K. Horii, H. Umemoto, A. Masuda, H. Matsumura, Thin Solid Films 395 (2001) 47.

[41] J. K. Holt, M. Swiatek, D. G. Goodwin, R. P. Muller, W.A. Goddard III, H. A. Atwater, Thin Solid Films 395 (2001) 29.

[42] H. L. Duan, G. A. Zaharias, S. F. Bent. Appl. Phys. Lett. 78 (2001) 1784.

[43] S. Tange, K. Inoue, K. Tonokura, M. Koshi, Thin Solid Films 395 (2001) 42.

[44] H. L. Duan, G. A. Zaharias, S.F. Bent, Thin Solid Films 395 (2001) 36.

[45] K. Tonokura, K. Inoue, M. Koshi, J. Non-Cryst. Solids 299-302 (2002) 25.

[46] J. K. Holt, M. Swiatek, D. G. Goodwin, H. A. Atwater, J. Appl. Phys. 92 (2002) 4803.

[47] H. Umemoto, T. Morimoto, M. Yamawaki, Y. Masuda, A. Masuda, H. Matsumura, Thin

Solid Films 430 (2003) 24.

[48] H. L. Duan, S. F. Bent, Thin Solid Films 485 (2005) 126.

[49] W. Zheng, A. Gallagher, Thin Solid Films 501 (2006) 21.

[50] W. Zheng, A. Gallagher, Thin Solid Films 516 (2008) 929.

[51] G. A. Zaharias, H. L. Duan, S. F. Bent, J. Vac. Sci. Technol. A 24 (2006) 542.

[52] X. M. Li, B. D. Eustergerling, Y. J. Shi, Int. J. Mass Spectrom. 263 (2007) 233.

[53] Y. Shi, X. Li, L. Tong, R. Toukabri, B. Eustergerling, Phys. Chem. Chem. Phys. 10 (2008) 2543.

[54] L. Tong, Y. J. Shi, Thin Solid Films 517 (2009) 3461.

[55] L. Tong, Y. J. Shi, J. Mass Spectrom. 45 (2010) 215.

[56] Y. J. Shi, X. M. Li, R. Toukabri, L. Tong, J. Phys. Chem. A 115 (2011) 10290.

[57] I. Badran, T. D. Forster, R. Roesler, Y. J. Shi, J. Phys. Chem. A 116 (2012) 10054.

[58] M. D. Buzaianu, V. I. Makarov, G. Morell, B. R. Weiner, Chem. Phys. Lett. 455 (2008) 26.

[59] D. W. Comerford, A. Cheesman, T. P. F. Carpenter, D. M. E. Davies, N. A. Fox, R. S. Sage, J. A. Smith, M. N. R. Ashfold, Yu. A. Mankelevich, J. Phys. Chem. A 110 (2006) 2868.

[60] H. Umemoto, T. Morimoto, M. Yamawaki, Y. Masuda, A. Masuda, H. Matsumura, J. Non-Cryst. Solids 338-340 (2004) 65.

[61] H. Umemoto, Y. Nishihara, T. Ishikawa, S. Yamamoto, Jpn. J. Appl. Phys. 51 (2012) 086501.

[62] H. Umemoto, Thin Solid Films http://dx.doi.org/10.1016/j.tsf.2014.10.015

[63] H. Umemoto, T. Kanemitsu, Y. Kuroda, Jpn. J. Appl. Phys. 53 (2014) 05FM02.

[64] A. C. G. Mitchell, M. W. Zemansky, Resonance Radiation of Excited Atoms, Cambridge University Press, London, 1934.

[65] H. Umemoto, K. Ohara, D. Morita, Y. Nozaki, A. Masuda, H. Matsumura, J. Appl. Phys. 91, (2002) 1650.

Table and Figure Captions

Table 1 Radical species produced on heated metal catalyst surfaces. H-atom production from H_2 is not included.

Fig. 1. Experimental (upper) and simulated (lower) spectra of OH in a pure H_2O system. The flow rate and the pressure were 1.50 sccm and 0.8 Pa, respectively. The Ir catalyst temperature was 2100 K. The laser intensity was low enough not to saturate the transitions. Assignments are shown for the P_1, Q_1, Q_2, and R_2 branches of the (0,0) band. The numbers are the total angular momentum quantum numbers exclusive of nuclear and electron spin. The rotational temperature was assumed to be 350 K in the simulation.

Table 1

Radical species produced on heated metal catalyst surfaces. H-atom production from H_2 is not included.

Material gas	Detected radical	Catalyst	Detection technique	Ref.
CH_4/H_2	CH_3	W	TDLAS [a]	[6]
CH_4/H_2	H, CH_3	W	TIMS [b]	[7]
CH_4/H_2	CH_3	W	REMPI [c]	[8]
CH_4/H_2	CH_3	W	REMPI	[9]
CH_4/H_2	CH_3	W	PA(Xe lamp) [d]	[10]
CH_4/H_2	CH_3	Ta	REMPI	[11]
C_2H_2/H_2	CH_3	W	PA(Xe lamp)	[12]
CH_4/H_2	CH_3	W	PA(Xe lamp)	[13]
CH_4/H_2	CH, CH_3	W	PA(Xe lamp)	[14]
CH_4/H_2, C_2H_2/H_2	H, CH_3	W	TIMS	[15]
CH_4/H_2	CH_3	W	CRDS [e]	[16]
CH_4/H_2	CH_3	W	CRDS	[17]
CH_4/H_2	CH_3	W	CRDS	[18]
CH_4/H_2	H, C, CH_3	W	PA (SR)	[19]
CH_4/H_2	CH_3	W	CRDS	[20]
CH_4/H_2, C_2H_2/H_2	H, CH_3	no data	REMPI/TOFMS [f], TIMS	[21]
CH_4/H_2	CH	W	CRDS	[22]
H_2, CH_4/H_2, C_2H_2/H_2	H, CH_3	Ta	REMPI	[23]
CH_4/H_2	CH	W, Re	CRDS	[24]
CH_4/H_2, C_2H_2/H_2	CH_3	Ta	REMPI	[25]
$CH_4/N_2/H_2$, $CH_4/NH_3/H_2$	H, CH_3, NH	Ta	REMPI, CRDS	[26]
CH_4/H_2, $CH_4/N_2/H_2$, $CH_4/NH_3/H_2$	H, CH_3	Ta	REMPI	[27]
CH_4/H_2	CH_3	W	TDLAS	[28]
CH_4/H_2	CH_3	no data	TDLAS	[29]
NH_3	H, NH, NH_2	W	PA(VUV), LIF [g]	[30]
NH_3	H, NH	W, Ru	PA(VUV), LIF, VUVLI F [h]	[31]
N_2	N	W	VUVLIF	[32]

N_2	N	W	VUVLIF	[33]
O_2/ H_2	H, O, OH	W	PA(VUV), LIF, VUVLIF, 2PLIF [i]	[34]
O_2, NO, N_2O, NO_2	O	Ir	PA(VUV), VUVLIF	[35]
H_2, O_2, O_2/H_2	H, O, OH	Ir	PA(VUV), LIF, VUVLIF, 2PLIF	[36]
H_2O, H_2O/O_2	H, O, OH	Ir	PA(VUV), LIF, VUVLIF, 2PLIF	[37]
SiH_4	H, Si, SiH_3	W	TIMS	[38]
SiH_4, SiH_4/H_2	Si, SiH	W	LIF	[39]
SiH_4, SiH_4/H_2	Si, SiH_3	W	LIF, CRDS	[40]
SiH_4	SiH_2, SiH_3	W	TIMS	[41]
SiH_4	Si, SiH_3	W	SPIMS [j]	[42]
SiH_4	H, Si, SiH_2, SiH_3	W, Ta, Mo	SPIMS, REMPI	[43]
SiH_4	Si, SiH_3	W	SPIMS	[44]
SiH_4	H, Si	W	REMPI	[45]
SiH_4	Si, SiH, SiH_2, SiH_3	W	TIMS	[46]
SiH_4/NH_3	NH, NH_2, SiH_3	W	LIF, CRDS	[47]
SiH_4	Si	W, Ta, Mo, Re	SPIMS	[48]
SiH_4	H, Si, SiH_3	W	TIMS	[49]
SiH_4	H, Si	W, Ta	TIMS	[50]
SiH_4, $(CH_3)SiH_3$, $(CH_3)_2SiH_2$, $(CH_3)_3SiH$, $(CH_3)_4Si$, 1,1-dimethyl-1-silacyclobutane	Si, CH_3	W, Re	SPIMS	[51]
$(CH_3)_4Si$	CH_3, $(CH_3)_3Si$	W	SPIMS	[52]
hexamethyldisilane	CH_3, $(CH_3)_3Si$, $(CH_3)_3SiSi(CH_3)_2$	W	SPIMS	[53]
1,1,3,3-tetramethyl -1,3-disilacyclobutane	CH_3, 1,1,3-trimethyl -1,3-disilacyclobutane-1-yl	W	SPIMS	[54]
1,1-dimethyl-1-silacyclobutane	CH_3, $(CH_3)_2Si$	W	SPIMS	[55]
$(CH_3)_3SiH$	CH_3, $(CH_3)_2SiH$, $(CH_3)_3Si$	W	SPIMS	[56]
1-methylsilacyclobutane	CH_3, CH_3SiH, silacyclobutane-1-yl	W	SPIMS	[57]

$H_2S/CH_4/H_2$	SH, CS	Re	CRDS	[58]
B_2H_6/H_2, $B_2H_6/CH_4/H_2$	H, B	Ta, Re	REMPI	[59]
HCN	H, CN	W	PA(VUV), LIF	[60]
PH_3	H, P, PH, PH_2	W	PA(VUV), LIF, VUVLIF	[61]
PH_3	P	W, Ta, Mo, Ir,	VUVLIF	[62]
P_4	P	W, Ta, Mo	VUVLIF	[63]

[a] tunable diode laser absorption spectroscopy

[b] threshold ionization mass spectrometry

[c] resonance-enhanced multiphoton ionization

[d] photo-absorption (Xe lamp, vacuum ultraviolet laser, or synchrotron radiation)

[e] cavity ringdown spectroscopy

[f] time-of-flight mass spectrometry

[g] laser-induced fluorescence

[h] vacuum ultraviolet laser-induced fluorescence

[i] two-photon laser-induced fluorescence

[j] single-photon ionization mass spectrometry

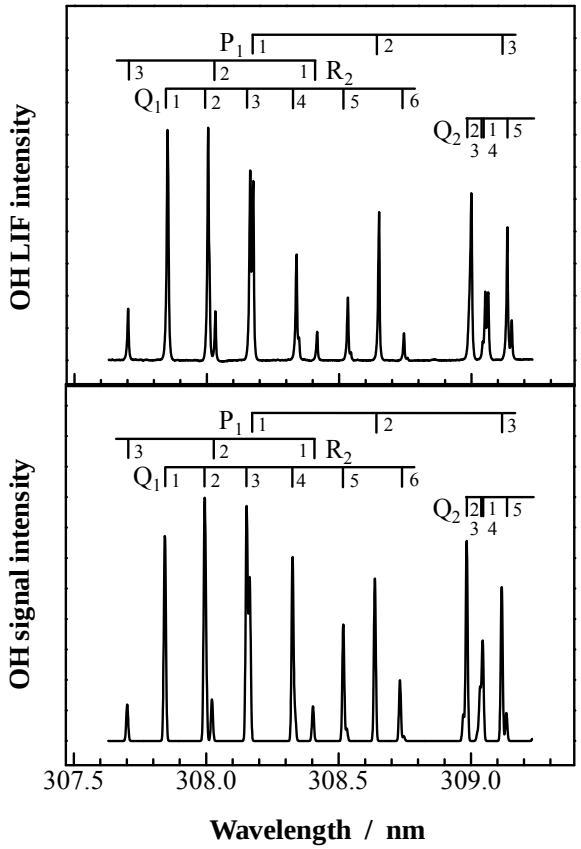

Fig. 1 H. Umemoto